Applied Composite Materials
https://doi.org/10.1007/s10443-024-10213-4

RESEARCH

On the Micro-Stress Fields in Fibre-Hybrid Polymer Composite Laminae with Periodic Microstructure Under Transverse Tension and Transverse Shear Loading

G. Romano[1] · Y. N. Rao[1] · C. Liu[1] · K. B. Katnam[1,3] · Z. Zou[1,3] · P. Potluri[2,3]

Received: 6 October 2023 / Accepted: 14 February 2024

Abstract
This paper investigates the effect of intra-laminar fibre hybridisation, *i.e.,* primary and secondary fibres within a matrix, on the homogenised properties and micro-stress fields in uni-directional polymer composite laminae. The study is focused on S-glass/epoxy laminae which are hybridised with secondary fibres (*e.g.,* polypropylene). Two-dimensional repeating unit cells (2D RUCs) with periodic microstructures are developed to conduct the micro-mechanical analyses under transverse tensile and transverse shear loading conditions. Uni-directional fibre-hybrid S-glass/epoxy laminae with different secondary fibres are studied by varying (a) the periodic microstructure and (b) the material properties of the constituent fibres to assess the effect of such geometric and material variations on the homogenised elastic lamina properties and intra-lamina micro-stress fields. The results show that intra-laminar fibre hybridisation significantly affects the elastic lamina properties and micro-stress fields. Notably, the presence of the secondary fibres significantly increases or reduces the stress fields in the matrix and at the fibre-matrix interfaces (i.e. normal and shears stress components)–depending on the microstructure and the stiffness of the secondary fibres–which could be explored to manipulate the damage modes and thus energy dissipation mechanisms.

Keywords Fibre-hybrid composites · Repeating unit cells · Homogenisation · And micro-stress fields

✉ K. B. Katnam
kali-babu.katnam@manchester.ac.uk

[1] Department of Mechanical, Aerospace and Civil Engineering, The University of Manchester, Manchester M13 9PL, UK

[2] Department of Materials, The University of Manchester, Manchester M13 9PL, UK

[3] Northwest Composites Centre, The University of Manchester, Manchester M13 9PL, UK

1 Introduction

The impact resistance and damage tolerance of conventional composite laminates, which depend on the failure and energy dissipation mechanisms at micro-, meso- and macro-scales, are the Achilles heel to ensure the structure safety and reliability due to the brittle behaviour of the constituents (*e.g.,* carbon fibres and epoxy matrix). Damage modes such as fibre-matrix de-bonding, matrix cracking, fibre breakage and delamination, can significantly influence the energy dissipation and load-carrying capacity of laminates [1]. To address some of the disadvantages of the conventional composite laminates, two or more fibres can be combined to produce fibre-hybrid composites (FHCs), such as inter-laminar (with different single fibre-based laminae) or intra-laminar (with more than one fibre-based laminae) hybrid laminate. The mechanical behaviour of fibre-reinforced composites not only depends on the constituent properties, microstructure, and fibre architecture but also be influenced by matrix hybridisation, fibre hybridisation and stacking sequence [2–7]. Hybrid composites (with matrix hybridisation and/or fibre hybridisation) can offer new opportunities to tailor the overall material properties and mechanical behaviour of laminates, *e.g.,* specific stiffness, specific strength, effective density, damage tolerance and impact resistance [8]. Recent experimental studies have demonstrated that an effective approach to enhance the impact performance of woven composite laminate is to use *fibre-hybrid systems* by combining either different fabric types (*i.e.,* hybrid layup) or different warp and fill yarns (*i.e.,* hybrid weave), or commingled fibres (*i.e.,* hybrid yarns) [9, 10]. Fibre-hybridization allows the fibres to store strain energy that would otherwise be used for crack propagation, resulting in improved damage tolerance [11–14]. Combining high-stiffness and high-strength fibres with low-stiffness and ductile fibres can create a composite with a good stiffness-toughness balance, which is challenging to achieve as strength and toughness are often mutually exclusive properties [15]. Yarn-level hybridization by combining low-stiffness and high-stiffness fibres has been successfully used to enhance damage tolerance compared to conventional composite laminates [11, 13, 14, 16]. The transverse properties of uni-directional composite lamina play a crucial role as intra-laminar transverse damage, *e.g.,* matrix cracking and fibre debonding, can significantly affect the damage evolution and failure of composite structures [17–19].

The relationship between the continuum properties of a material neighbourhood and its microstructure and micro-constituents is important for heterogeneous materials, especially for fibre-reinforced polymer composites with heterogeneity at the microscale. The notion of a representative volume element, or repeating unit cell, is used as the physical basis for the transition from the microscale to the macroscale, and the associated boundary-value problem is formulated in terms of field variables by imposing traction and/or displacement boundary conditions. Computational micromechanics plays a major role in understanding the deformation processes at the microscale as well as in estimating the homogenised properties of composite laminae with intra-laminar fibre hybrid microstructure. Repeating unit cells (RUCs) have been widely used to predict the homogenised elastic properties of uni-directional composites [20–22] and to investigate failure initiation under mechanical, thermal and thermo-mechanical loading [23, 24]. The influence of inter-fibre distance on the interface properties for irregular and hexagonal packing of fibres of a uni-directional carbon/epoxy composite was studied by Hojo et al. [23], and it was shown that when the fibres were at their minimum inter-fibre distance and almost aligned with the loading direction (*i.e.* $\theta \leq 30°$), the tensile interfacial normal stress was significantly high. Furthermore, it was observed in unidirectional carbon/epoxy composites that thermal

residual stresses resulting from the cooling step at the end of the curing cycles reduced the tensile interfacial normal stress under thermo-mechanical loading in comparison with solely mechanical loading.

These localized deformation and fibre-matrix interface fractures are tell-tale signs of the mechanisms of initial transverse failure. Another research conducted by Jin et al. employed RUC and RVE models to understand the effect of fibre array irregularity on thermal residual stresses [24]. In contrast, only a limited amount of research attention has been given to intra-laminar or intra-two/yarn fibre-hybrid laminates using RUC or RVE models [25]. Recently, Banerjee and Sankar [26] investigated the micro-mechanical behaviour of fibre-hybrid carbon/E-glass/epoxy composite lamina using representative volume elements with carbon and E-glass fibres with equal fibre diameter arranged randomly in a hexagonal packing pattern. The model was shown to have successfully predicted the elastic and strength properties of the intra-laminar fibre-hybrid composites [26]. However, the effect of inter-fibre distance and secondary fibre stiffness on the micro-stress fields were not accounted for in the models. Moreover, several analytical models were developed to predict the elastic properties of non-hybrid uni-directional composites [27]. Banerjee and Sankar [26] used the rule of hybrid mixture to predict the longitudinal elastic moduli and major Poisson's ratio, and a modified Halpin–Tsai equation to predict the transverse tension and transverse shear elastic moduli. However, the analytical model such as modified Halpin–Tsai requires curve-fitting parameters, depending on fibre packing and fibre type [26]. Overall, the effects of intra-laminar or intra-two/yarn fibre hybridisation, micro-structure and constituent properties on the behaviour of fibre-hybrid composites are not well understood and thus need more research attention.

In this paper, fibre-hybrid uni-directional laminae with periodic microstructures are investigated using repeating unit cell (RUC) models to understand the influence of intra-laminar fibre hybridisation on the homogenised elastic lamina properties and intra-laminar micro-stress fields. The RUC models are used to study the role of the secondary fibre stiffness and the inter-fibre distance between the primary and secondary fibres on the fibre-matrix interface and matrix micro-stress fields. A modified transverse diagonal packing scheme is adopted to accommodate fibre-hybridization. The study mainly focuses on S-glass/polypropylene/epoxy laminae under transverse tension and transverse shear loading to understand the matrix-dominant behaviour of such fibre-hybrid composite laminates. The predicted effective transverse elastic moduli are compared against Mori-Tanaka [28, 29] and Chamis [30, 31] analytical models for conventional unidirectional composite laminae. The validated RUC models are used to conduct parametric studies and the results are presented.

2 Methodology

2.1 RUC Modelling

Fibre-hybrid uni-directional laminae with periodic microstructures are analysed using two-dimensional repeating unit cell (2D RUC) models to predict the homogenised elastic lamina properties and micro-stress fields under transverse tension and transverse shear. As the interaction between the constituents at the micro-scale can play a crucial role in fibre-hybrid polymer composites, the effects of fibre hybridisation, constituent properties and periodic microstructure are investigated using the RUC approach. The RUC is the smallest idealised

unit cell capable of representing the behaviour of the whole microstructure [32]. In this study, a 2D RUC model is implemented to accommodate fibre hybridization by considering a diagonal square packing for the periodic microstructure [33]. In Fig. 1, a hybrid laminate with intra-laminar fibre hybridisation, featuring primary fibres (S-glass fibres) and secondary fibres (Fig. 1a), and a 2D RUC with a periodic microstructure with diagonal square packing for the micromechanical analysis (Fig. 1b) are shown. The coordinate system (x_i) in Fig. 1 is aligned with the principal material coordinate system of the uni-directional fibre-hybrid lamina. Moreover, to study the effect of the inter-fibre distance between fibres, as shown in Fig. 1b, the position of the centre of the middle (secondary) fibre is varied from the centre of the RUC. The fibre eccentricity is defined by two components: an eccentricity distance, δ_e, and an eccentricity angle, θ_e, which is measured counter-clockwise in degrees about the x_2-axis. Furthermore, Fig. 1b illustrates the interfacial normal, σ_n, and shear, τ_{nt}, stresses at the fibre-matrix interface of the secondary fibre at the centre and the S-glass fibres at the corners. To simplify the model, the fibres within the lamina are assumed continuous, homogeneous, isotropic, and defect-free with circular cross-sections. The matrix is assumed homogeneous, isotropic, and void-free. The fibres are also assumed to have a perfect fibre-matrix interface. The variation in the material properties and diameter of each fibre type is assumed to be negligible, and the fibres and matrix are linear elastic. The diameters of the primary (S-glass) and secondary fibres are assumed to be 10 µm. The total fibre volume fraction (V_f), which is the sum of the primary fibre volume fraction (V_{fP}) and the secondary fibre volume fraction (V_{fS}), is assumed to be 0.6 in all the laminae analysed. For example, the S-glass fibre volume fraction ($V_f = V_{fP} = V_{fG}$) in S-glass/epoxy lamina is 0.6; whereas the combined S-glass and PP fibre volume fraction is 0.6 in S-glass/PP/epoxy lamina ($V_f = V_{fG} + V_{fPP} = 0.6$). The RUC size ($L$) is determined from the total fibre volume fraction, *i.e.*, $V_f = A_f/A_{RUC}$, where A_f is the total cross-sectional area of the primary and secondary fibres (*i.e.*, $2\pi r_{fP}^2$, with r_{fP}, the radius of primary fibre) and A_{RUC} is the RUC area (*i.e.*, L^2)—thus $L = r\sqrt{2\pi/V_f}$.

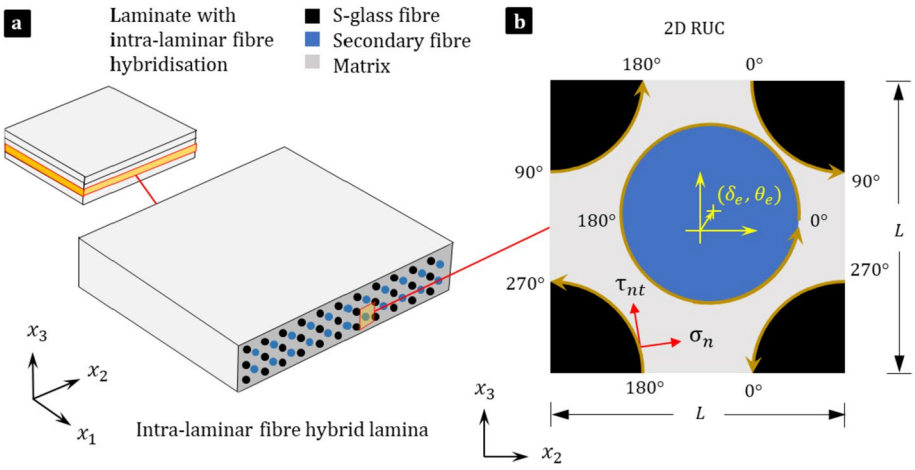

Fig. 1 The modelling approach used: **a** a laminate with intra-laminar fibre-hybrid lamina, and **b** a 2D RUC of S-glass/secondary-fibre/matrix lamina with diagonal square packing (with fibre eccentricity)

The RUC model is implemented in *ABAQUS/Standard*. A *Python* script is used, and the displacement-based periodic boundary conditions (PBCs) are imposed by generating matching nodes on the opposite edges. Considering plane strain conditions, the 2D RUC is analysed with a quad-dominant mesh with CPE4R (a 4-node bilinear plane strain element with reduced integration) and CPE3 (a 3-node linear plane strain element with full integration) elements. Considering the convergence of the homogenised elastic lamina properties, a mesh convergence study is conducted to identify a suitable element size/mesh.

The material properties of the constituents and the diameter of the fibres are given in Table 1. The fibres used in the study are S-glass [34, 35] and polypropylene (PP) [36, 37], while the matrix is *Araldite LY564/Aradur 2954*, a two-part epoxy resin [38]. All the constituent materials are assumed to be isotropic and linear elastic.

2.2 Periodic Boundary Conditions

The unweighted volume averages of the micro-stresses and micro-strains within the RUC can be used to estimate the homogenised properties of fibre-hybrid laminae. The estimated properties, however, are dependent on the type of boundary conditions imposed on the RUCs. The upper and lower bounds of the homogenised properties are provided by the boundary conditions of linear displacement (uniform macro-strain) and uniform traction (uniform macro-stress). When the same average strain is considered for each case, the strain energies predicted by imposing uniform traction, periodic displacement, and linear displacement boundary conditions satisfy the inequality $W_t \leq W_p \leq W_u$ (where W_t, W_p, W_u are the strain energies obtained by imposing uniform traction, periodic displacement, and linear displacement boundary conditions, respectively). Additionally, the PBCs guarantee continuity between adjacent RUCs and ensure that the RUC behaves as the entire medium (*i.e.,* composite lamina). Thus, the RUC is considered the smallest idealised unit cell able to behave as the infinite medium [39]. To apply PBC, the mesh on opposite edges must have the same number of nodes and the nodes must be perfectly aligned [20, 40]. Moreover, the geometry of the RUC must be periodic, if a partial fibre is on an edge, the remaining part must be on the opposite edge to form a complete fibre. The displacement-based periodic boundary conditions (PBCs) are applied to the RUC model using *Equation* constraints in *ABAQUS/Standard* [41–43], and the process is automatized by using a *Python* script. The periodic displacement conditions are imposed by using Eq. 1 [20, 44, 45]. Although applying linear displacement boundary conditions generally does not guarantee periodic traction conditions (similarly, applying uniform traction conditions does not guarantee periodic displacement conditions) at the boundaries, it can be shown that periodic displacement conditions guarantee periodic traction conditions.

$$u_i(\boldsymbol{x} + \Delta \boldsymbol{x}) - u_i(\boldsymbol{x}) = \widehat{\varepsilon}_{ij} \Delta x_j \quad (i,j = 1, 2, 3) \tag{1}$$

Table 1 The material properties of the fibres and matrix used in the RUC models of S-glass/epoxy and S-glass/PP/epoxy fibre-hybrid laminae [34–38]

	$E_{11}=E_{22}=E_{33}$ [GPa]	$G_{12}=G_{13}=G_{23}$ [GPa]	$v_{12}=v_{13}=v_{23}$	ρ [g/cm^3]	d [μm]
S-glass	87.0 ± 1.00	35.40 ± 0.10	0.23 ± 0.02	2.46 ± 0.03	10
Polypropylene	1.20 ± 0.10	0.42 ± 0.03	0.42 ± 0.04	0.90 ± 0.05	10
Epoxy	2.55 ± 0.10	0.94 ± 0.03	0.35 ± 0.04	1.15 ± 0.05	-

In Eq. 1, u_i is the displacement in the x_i direction, $\boldsymbol{x} + \Delta\boldsymbol{x}$ and $\boldsymbol{x}$ are the position vectors of the points on the opposite faces of the RVE, and $\widehat{\varepsilon}_{ij}$ is the macro-strain components. In the case of a 2D domain as in Fig. 2, the application of PBCs can be defined by Eq. 2 [20, 41, 42]:

$$u_i^{n^+|\boldsymbol{\Gamma}_{2-3}} - u_i^{n^-|\boldsymbol{\Gamma}_{1-4}} = u_i^{n_2} \quad u_i^{n^+|\boldsymbol{\Gamma}_{3-4}} - u_i^{n^-|\boldsymbol{\Gamma}_{1-2}} = u_i^{n_4} \quad (i = 2, 3) \tag{2}$$

In Eq. 2, $u_i^{n^+|\Gamma_{2-3}}$ is the displacement at node n^+ on the edge Γ between the nodes n_2 and n_3; $u_i^{n^-|\Gamma_{1-4}}$ is the displacement at node n^- on the edge Γ between the nodes n_1 and n_4; $u_i^{n^+|\Gamma_{3-4}}$ is the displacement at node n^+ on the edge Γ between the node n_3 and n_4; and $u_i^{n^-|\Gamma_{1-2}}$ is the displacement at node n^- on the edge Γ between the node n_1 and n_2. Moreover, $u_i^{n_2}$ and $u_i^{n_4}$ are the displacements at the master nodes n_2 and n_4 to apply the period displacements. Thus, for each pair of opposite nodes, the periodic displacement is equal to the displacement at the master node n_i. The domain is meshed such that all the nodes n^- and n^+ on the opposite edges are perfectly aligned (see Fig. 2c). Figure 2 shows the boundary conditions employed to implement transverse tension (in the x_2-direction) and transverse shear loading conditions. In both cases, the node n_1 is pinned (*i.e.*, $u_2^{n_1} = 0$ and $u_3^{n_1} = 0$) to avoid the rigid body motions. For the case of transverse tension along the x_2-direction, the displacement is constrained at node n_4 (*i.e.*, $u_2^{n_4} = 0$) and node n_2 (*i.e.*, $u_3^{n_2} = 0$) to prevent any rotation and guarantee contraction in the x_3-direction, while the periodic displacement in the x_2-direction is applied to the node n_2 (*i.e.*, $u_2^{n_2} = \delta$) as shown in Fig. 2a. For the case of transverse shear, a displacement $(\delta/2)$ is applied to the node n_2 in the x_3-direction (*i.e.*, $u_3^{n_2} = \delta/2$), and to the node n_4 in the x_2-direction (*i.e.*, $u_2^{n_4} = \delta/2$), see Fig. 2b. Furthermore, if a node belongs to the adjacent edges (node n_3 in this case), the periodicity is applied to the node based on one of the edges. Thus, if the node n_3 is assumed to belong to the edge Γ_{3-4}, it cannot belong to the edge Γ_{2-3}, and vice-versa [46, 47].

2.3 Homogenization

The homogenized properties of the lamina are determined by applying a macro-strain (*i.e.*, $\widehat{\varepsilon}_{ij}$) state (displacement applied to the master nodes) [22], and then calculating the unweighted volume average of the unknown variables within the repeating unit cell (RUC). By applying Gauss's divergence theorem and considering the condition $\sigma_{ij,j} = 0$ for the

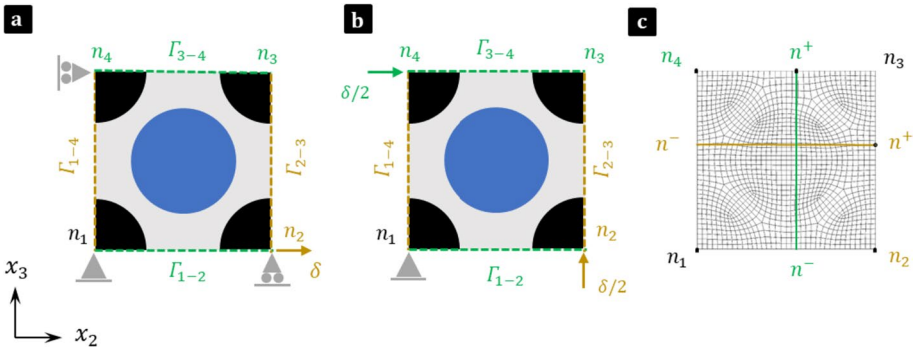

Fig. 2 The boundary conditions: **a** transverse tension in the $\mathbf{x}_2$-direction, **b** transverse shear, and **c** the periodic mesh for the 2D RUC model

micro-stress field (*i.e.,* divergence-free), the unweighted volume averages of the micro-stress is obtained by using Eq. 3, from the reaction forces at the reference (master) nodes, which are used to impose the periodic boundary conditions. Similarly, the unweighted volume average of the micro-strain is obtained by using Eq. 4, whether the displacements applied at the control nodes to impose the macrostrain conditions can be used to calculate the macrostrain components. In Eqs. 3–4, $\widehat{\sigma}_{ij}$ is the macro-stress, $\widehat{\varepsilon}_{ij}$ is the macro-strain, Ω is the RUC volume, $\overline{n}_i$ is the outward normal at the boundary, $\left(F_i\right)_j$ is the resultant force on the surface with the outward normal in the x_j-direction) at the reference node in the x_i-direction, and Υ_j is the area of the boundary surfaces with the outward normal in the x_j-direction.

$$\widehat{\sigma}_{ij} = \frac{1}{\Omega}\int_{\Omega} \sigma_{ij}\, \mathrm{d}\Omega = \int_{\partial\Omega=\Upsilon} \sigma_{ik}\overline{n}_k x_j \mathrm{d}\Upsilon = \frac{\left(F_i\right)_j}{\Upsilon_j} \quad \text{(no summation over the index } j\text{)} \tag{3}$$

$$\widehat{\varepsilon}_{ij} = \frac{1}{\Omega}\int_{\Omega} \varepsilon_{ij} d\Omega = \frac{1}{2\Omega}\int_{\partial\Omega=\Upsilon} (u_i \overline{n}_j + u_j \overline{n}_i) d\,\Upsilon \tag{4}$$

Using a 3D RUC model, the homogenised elastic lamina properties (*i.e.,* $\widehat{E}_{11}$, $\widehat{E}_{22}$, $\widehat{E}_{33}$, $\widehat{G}_{12}$, $\widehat{G}_{13}$, $\widehat{G}_{23}$, $\widehat{\nu}_{12}$, $\widehat{\nu}_{13}$, $\widehat{\nu}_{23}$) can be obtained from $\widehat{\sigma}_{ij}$ and $\widehat{\varepsilon}_{ij}$. However, as plane strain conditions are used for the 2D RUC model to study the transverse tensile and transverse shear behaviour of hybrid laminae, the homogenised properties $\widehat{E}_{22}$, $\widehat{E}_{33}$, $\widehat{G}_{23}$ and $\widehat{\nu}_{23}$ are analysed in this work. The specific transverse lamina elastic moduli $\widehat{E}_{22}/\widehat{\rho}$ and $\widehat{G}_{23}/\widehat{\rho}$ are then obtained (where $\widehat{\rho}$ is the effective density of the lamina). Using a square RUC (each edge Γ_i has the same dimension, L) with unit thickness, the transverse elastic properties and density of the lamina are determined by using Eq. 5. The effective density is determined from the densities of the micro-constituents using Eq. 5d, where ρ_m is the matrix density, ρ_{fi} is the fibre density and V_{fi} is the fibre volume fraction ($i = P, S$; for the primary and secondary fibres).

$$\widehat{E}_{22} = \frac{\widehat{\sigma}_{22}}{\widehat{\varepsilon}_{22}} = \frac{\left(R_2\right)_2}{u_2^{n_2}} \tag{5a}$$

$$\widehat{G}_{23} = \frac{\widehat{\sigma}_{23}}{\widehat{\varepsilon}_{23}} = \frac{\left(R_2\right)_3}{(u_3^{n_2} + u_2^{n_4})} \tag{5b}$$

$$\widehat{\nu}_{23} = -\frac{\widehat{\varepsilon}_{33}}{\widehat{\varepsilon}_{22}} = -\frac{u_2^{n_4}}{u_3^{n_2}} \tag{5c}$$

$$\widehat{\rho} = \rho_m\left(1 - \sum V_{fi}\right) + \sum \rho_{fi} V_{fi} \quad (i = P, S) \tag{5d}$$

2.4 Model Validation

To verify and validate the 2D RUC model, non-heterogeneous (*i.e.,* the same material properties are assigned to the matrix and fibres) and non-hybrid lamina (*i.e.,* the same material properties are assigned to the primary and secondary fibres) conditions are considered for

Table 2 The comparison of the homogenised transverse properties obtained from the RUC model for a fibre volume fraction of 0.6 with the data Li [22]. The fibre and matrix properties are taken from Li [22]

	2D RUC model	Li [22]	Hashin and Rosen's theory [22]	
			Lower bound	Upper bound
$\hat{E}_{22}$ *(GPa)*	2.619 (+2%)	2.562	2.538	3.015
$\hat{G}_{23}$ *(GPa)*	1.340 (0%)	1.34	0.91	1.178
v_{23}	0.432 (+8%)	0.401	0.28	0.394

the periodic microstructure used. Subsequently, the non-heterogeneous condition is used to verify the model as the micro-stress and micro-strain must agree with the macro-stress and macro-stain, whereas the homogenised properties must agree with the material properties assigned to the micro-constituents [22]. Additionally, the non-hybrid condition is used to validate the RUC model with diagonal square packing. The variation in the homogenised properties, $\widehat{E}_{22}$ and $\widehat{v}_{23}$, are compared with those estimated by Li [22] (*i.e.,* with a 3D model) and with the upper and lower bounds by Hashin and Rosen's theory in Table 2. The % variation in Table 2 is relative to the estimations by Li [22], where the fibres are assumed to be isotropic with $E = 10$ GPa and $\nu = 0.2$ and the matrix is isotropic with $E = 1$ GPa and $\nu = 0.3$. The higher values of $\widehat{E}_{22}$ and $\widehat{v}_{23}$ compared to Li [22], who used a 3D Model are attributed to the 2D plane strain assumption employed. However, it's important to note that this assumption has no effect on $\widehat{G}_{23}$.

3 Results and Discussion

3.1 The Homogenised Elastic Properties of Fibre-hybrid Laminae

The homogenised elastic lamina properties are calculated using the RUC model for non-hybrid (S-glass/epoxy) and non-hybrid (S-glass/secondary/epoxy) laminae and presented in Fig. 3. As shown in Fig. 3a, to study the effect of the secondary fibre stiffness (E_{fS}) on the homogenised properties of fibre-hybrid laminae, S-glass/epoxy lamina

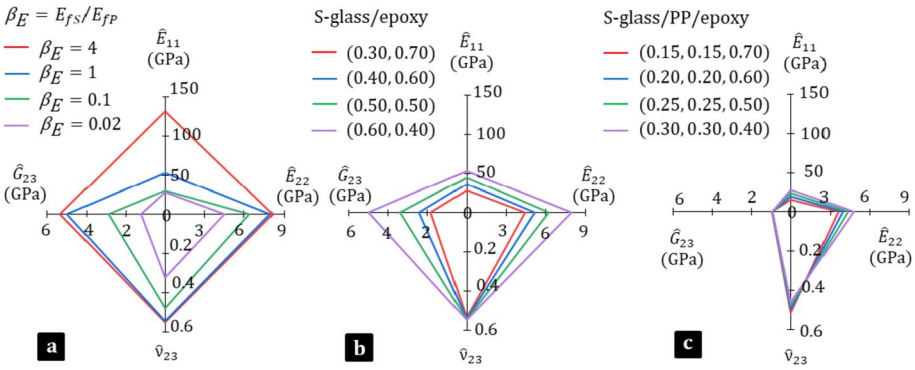

Fig. 3 The comparison of the homogenised elastic lamina properties: **a** S-glass/epoxy with different secondary fibres with $\left(V_{fG}, V_{fS}, V_m\right) = (0.3, 0.3, 0.4)$ and β_E from 4 to 0.02, **b** S-glass/epoxy with different volume fractions, and **c** S-glass/PP/epoxy with different volume fractions

Table 3 The secondary fibre stiffness in comparison with that of S-glass fibre

$\beta_E = E_{fs}/E_{fG}$	4	1	0.1	0.02
E_{fS} (Gpa)	348	87	8.7	1.74

with secondary fibres, with $\left(V_{fG}, V_{fS}, V_m\right) = (0.3, 0.3, 0.4)$, is analysed. The ratio of the secondary fibre stiffness (E_{fS}) and the primary fibre stiffness (E_{fP}, in this case, S-glass fibres, thus E_{fG}) is denoted as β_E. The Poisson's ratios of the primary and secondary fibres are assumed to be equal. Table 3 shows the variation in β_E, and the secondary fibre stiffness, E_{fS}, considered. For $\beta_E = 4$, the secondary fibre stiffness is significantly higher than that of the primary fibre (S-glass). With $\beta_E = 1$, it represents the baseline lamina (as the secondary fibre stiffness is equal to the primary fibre stiffness). Moreover, for $\beta_E = 0.02$, the secondary fibre stiffness is lower than that of the matrix, representing a fibre-hybrid lamina such as S-glass/PP/epoxy. The homogenised properties of fibre-hybrid lamina in Fig. 3a show that the stiffness of the secondary fibre plays a significant role. The homogenised transverse properties (*i.e.,* $\widehat{E}_{22}, \widehat{G}_{23}$ and $\hat{\nu}_{23}$) are calculated by the 2D RUC model and the homogenised longitudinal modulus ($\widehat{E}_{11}$) is estimated by the rule of mixture. Moreover, the homogenised properties of S-glass/epoxy lamina and S-glass/PP/epoxy, with varying fibre volume fraction, are shown in Fig. 3b, c, respectively. From Fig. 3b, c, it is seen that replacing some of the primary fibre content (S-glass) with the low stiffness secondary fibre content (*i.e.,* PP fibres) significantly affects the homogenised properties, especially the transverse shear modulus. As the lamina effective density is affected by the primary and secondary fibre contents, the specific elastic moduli (*i.e.,* $\widehat{E}_{11}/\hat{\rho}, \widehat{E}_{22}/\hat{\rho}$ and $\widehat{G}_{23}/\hat{\rho}$) are calculated and shown in Fig. 4a, b for S-glass/epoxy and S-glass/PP/epoxy laminae. The specific elastic moduli of S-glass/epoxy and S-glass/PP/epoxy lamina are considerably affected by the primary and secondary fibre contents and that the homogenised properties can be tailored by varying fibre types and hybridisation. It is worth noting that the homogenised properties could depend on the periodic microstructure and lead to transverse anisotropy.

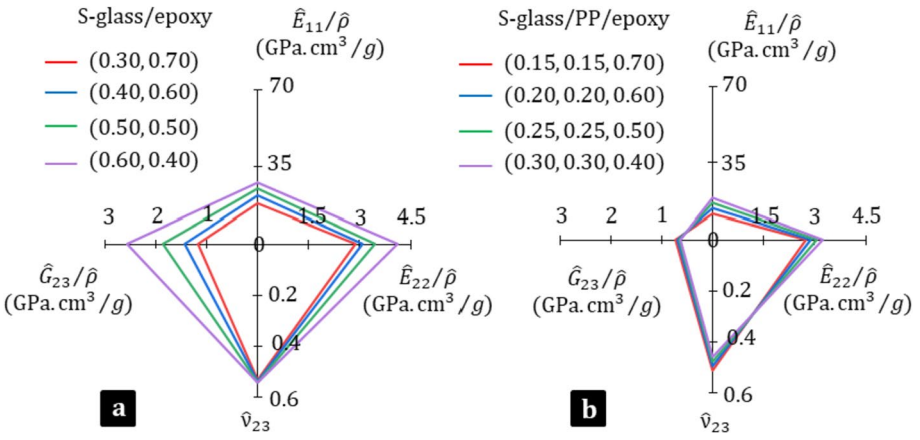

Fig. 4 The comparison of the specific homogenised elastic lamina properties: **a** S-glass/epoxy with different with different volume fractions, and **b** S-glass/PP/epoxy with different volume fractions

3.2 Fibre-hybrid Laminae Under Transverse Tension and Transverse Shear

3.2.1 The Effect of Secondary Fibre Stiffness on Micro-stress Fields

To study the effect of the secondary fibre stiffness (E_{fS}) on the micro-stress fields in fibre-hybrid laminae, S-glass/epoxy lamina with secondary fibres, with $\left(V_{fG}, V_{fS}, V_m\right) = (0.3, 0.3, 0.4)$, is analysed under transverse tension and transverse shear loading, and the von Mises matrix stress distributions as a measure of the local matrix stress state (normalized with the macro stress component applied, *i.e.,* $\sigma_{vM}/\hat{\sigma}_{22}$ and $\sigma_{vM}/\hat{\sigma}_{23}$) are shown in Fig. 5. The ratio of the secondary fibre stiffness (E_{fS}) and the primary fibre stiffness (E_{fP}, in this case, S-glass fibres, thus E_{fG}) is varied (*i.e.,* β_E from 4 to 0.02).

The variations in the von Mises matrix stress distribution with varying secondary fibre stiffness, in comparison with that of the baseline (*i.e.,* S-glass/epoxy lamina, with $\beta_E = 1$), are shown in Fig. 5a–h. First, the normalized von Mises matrix stress distributions ($\sigma_{vM}/\hat{\sigma}_{22}$) under transverse tension are presented in Fig. 5a–d. Figure 5a shows that a secondary (middle) fibre that is significantly (400%) stiffer than the S-glass (corner) fibre (*i.e.,* $\beta_E = 4$) only marginally alters the micro-stress distribution within the matrix, when compared to that of the baseline (*i.e.,* S-glass/epoxy lamina, Fig. 5b). When $\beta_E =$

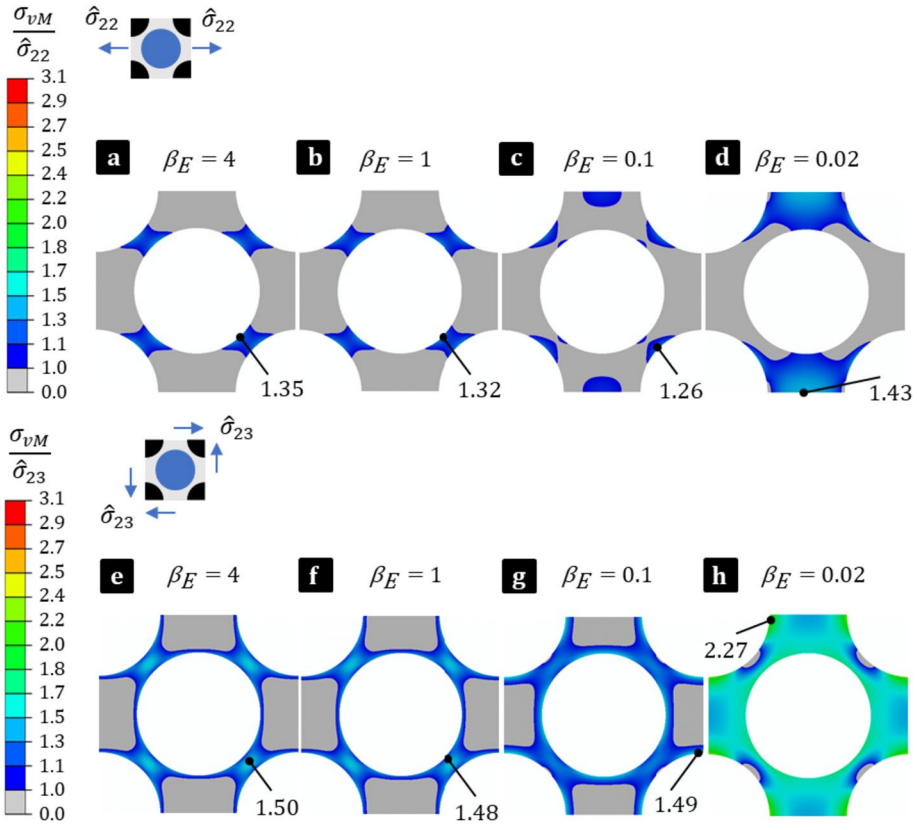

Fig. 5 The normalised von Mises matrix stress distribution **a–d** under transverse tension and **e–f** under transverse shear for different β_E (i.e., the primary (S-glass) fibre stiffness to the secondary fibre stiffness ratio)

0.1 (Fig. 5c), *i.e.,* the secondary fibre stiffness is significantly lower than that of the primary fibre, but higher than that of the matrix, the normalised von Mises stress distribution is considerably altered, yet only a small decrease in the maximum normalised stress (~5%) is observed. The maximum normalised stress is not at the minimum inter-fibre distance. When $\beta_E = 0.02$ (see Fig. 5d), *i.e.,* the secondary fibre stiffness is lower than that of the matrix, the normalised von Mises stress distribution is significantly altered, but an increase of only ~8% in the maximum normalised stress is seen compared to that of the baseline lamina. The maximum stress occurred at the minimum inter-fibre distance between the S-glass fibres (which are the stiffer fibres). Next, Fig. 5e–h show that the normalized von Mises matrix stress distributions under transverse shear ($\sigma_{vM}/\widehat{\sigma}_{23}$). Figure 5e shows that a secondary middle fibre that is significantly (400%) stiffer than the corner S-glass fibres (*i.e.,* $\beta_E = 4$) has negligible effect on the matrix micro-stress distribution compared to that of the baseline lamina (Fig. 5f). Similarly, a secondary middle fibre, with significantly lower stiffness than that of the S-glass fibre (*i.e.,* $\beta_E = 0.1$), also has insignificant influence on the matrix stress distribution. In contrast, from Fig. 5h, it is seen that a secondary fibre, with lower stiffness than that of the matrix ($\beta_E = 0.02$) significantly increases (~53% higher than that is in the baseline, Fig. 5f) the maximum normalised matrix stress and significantly alters the stress distribution within the matrix. The maximum normalised matrix stress occurs at the shortest distance between the stiffer fibres, aligning with the loading direction [23]. Thus, the presence of a secondary fibre with a significantly low stiffness ($E_{fS} = 1.74$ GPa), compared to the primary (S-glass) fibre ($E_{fG} = 87$ GPa) and the matrix ($E_m = 2.55$ GPa), is seen to induce a large increase in the normalised matrix stress under transverse tension as well as transverse shear conditions, when compared to that of the baseline (S-glass/epoxy lamina). This could be attributed to the increased load-bearing role of the matrix. When the secondary fibre stiffness is higher than that of the matrix ($E_{fS} = 8.7$ GPa), but lower than that of the primary (S-glass) fibre, it is seen to redistribute the matrix stresses and consequently reduce the normalised peak matrix stress (as in Fig. 5c, g compared to Fig. 5b, f). In general, these observations emphasize the importance of the secondary fibre stiffness in tailoring the macroscopic properties and the microscopic behaviour of fibre-hybrid laminae—and thus on the structural behaviour of such hybrid laminates.

Figure 6 shows the normalized fibre-matrix interfacial normal and shear stresses under transverse tension and shear (*i.e.,* $\sigma_n/\widehat{\sigma}_{22}$, $\tau_{nt}/\widehat{\sigma}_{22}$, $\sigma_n/\widehat{\sigma}_{23}$ and $\tau_{nt}/\widehat{\sigma}_{23}$). The normal and shear stress components are shown in counterclockwise (from 0° to 90°) at the fibre-matrix interface for the top right corner (primary) fibre and the middle (secondary) fibre. In Fig. 6a, $\sigma_n/\widehat{\sigma}_{22}$ for the top right corner (S-glass) fibre is shown. When the secondary fibre stiffness is equal to or higher than that of the S-glass fibre (*i.e.,* $\beta_E = 1$ and 4), the maximum normalised normal stress, $\sigma_n/\widehat{\sigma}_{22}$, is at $\theta = 0°$, which is aligned to the loading direction, and a second peak is at $\theta \approx 45°$, where the inter-fibre distance is a minimum [23]. The maximum normalised normal stresses for $\beta_E = 4$, 1, 0.1 and 0.02 are 0.82, 0.86, 1.15 and 1.71, respectively, showing that the normal stress at the primary fibre-matrix interface increases when the secondary fibre stiffness is decreased. For $\beta_E = 0.1$ and 0.02, the maximum normalised normal stress is at $\theta = 0°$, *i.e.,* at the shortest inter-fibre distance between the primary (stiffer) fibres. It occurs as the middle (secondary) fibre stiffness is lower than that of the corner (primary) fibre, while the loading is normal to the fibre-matrix interface at $\theta = 0°$. Moreover, for $\beta_E = 0.1$ and 0.02, the maximum normalised normal stress is higher by ~40% and ~110%, comparing with the baseline lamina ($\beta_E = 1$).

In Fig. 6b, the normalized interfacial normal stress $\sigma_n/\widehat{\sigma}_{22}$ for the secondary fibre is shown. It is evident that as the secondary fibre stiffness decreases the normalised normal

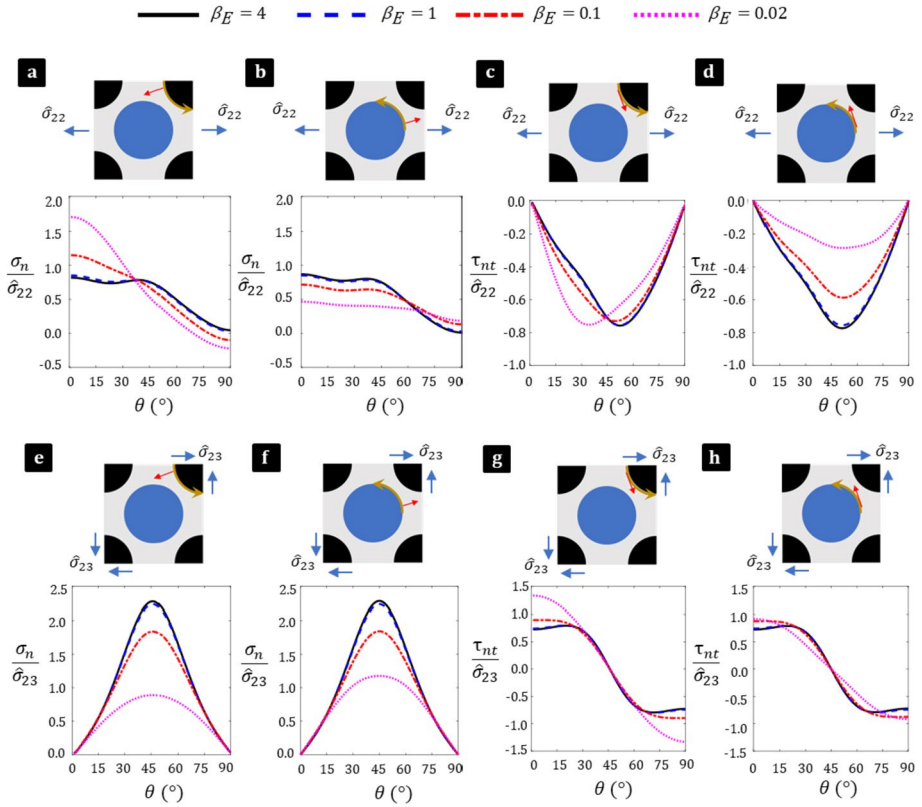

Fig. 6 The normalised normal and shear stress stresses under transverse tension and transverse shear at the primary (S-glass) and secondary fibre interfaces, for different secondary to S-glass fibre stiffness ratios β_E

stress at the secondary fibre-matrix interface decreases; and the interface normal stress is not amplified. Figure 6c shows the normalized interfacial shear stress ($\tau_{nt}/\hat{\sigma}_{22}$) for the corner (S-glass) fibre. The maximum normalised shear stresses are comparable (~0.8) for $\beta_E = 4$, 1, 0.1, and 0.02, although the location of the maximum shear stress moves with varying the secondary fibre stiffness. Figure 6d shows that the maximum normalised shear stress at the secondary fibre interface considerably decreases—from ~0.8 for $\beta_E = 4$, 1 to ~0.25 for $\beta_E = 0.02$. Moreover, Fig. 6e–h shows the normalized interfacial normal and shear stresses under transverse shear (*i.e.,* $\sigma_n/\hat{\sigma}_{23}$ and $\tau_{nt}/\hat{\sigma}_{23}$) for the primary (S-glass) and secondary fibres. From Fig. 6e–f, it is seen that the maximum normalised normal stress ($\sigma_n/\hat{\sigma}_{23}$) for the S-glass and secondary fibres occurs at $\theta = 45°$. Notably, the maximum normal stress for $\beta_E = 0.02$ is ~65% lower than the maximum normal stress for $\beta_E = 1$ at the S-glass fibre interface, and the maximum normal stress at the secondary fibre decreases by ~50% for $\beta_E = 0.02$. Figure 6g shows that the absolute normalised shear stress at the S-glass fibre for $\beta_E = 0.02$ is significantly higher (~80%) when compared to that of the baseline ($\beta_E = 1$), with peak stresses at $\theta = 0°$ and 90°. In addition, Fig. 6h shows that, for $\beta_E = 0.1$ and 0.02, the normalised shear stresses at the secondary fibre are higher than those are for $\beta_E = 4$ and 1. Therefore, the presence of a low-stiffness secondary fibre in S-glass/secondary/epoxy lamina under transverse tension and transverse

shear could influence S-glass fibre de-bonding. The low-stiffness secondary fibres could de-bond first, especially when the fibre interface strength is low, and influence micro-stress redistribution—consequently, micro-damage mechanisms and energy dissipation. These observations can have important implications on the strength and damage tolerance of composite structures, as supported by the experimental observations made from the impact and post-impact studies on E-glass/PP/epoxy and S-glass/PP/epoxy composite laminates with intra-yarn hybridization [11, 13, 14].

3.2.2 The Effect of Fibre Eccentricity on Micro-stress Distribution Under Transverse Tension

The influence of fibre eccentricity is investigated in two types of composite laminae: non-hybrid S-glass/epoxy and fibre-hybrid S-glass/PP/epoxy. A total fibre volume fraction of 0.6 (*i.e.,* $V_{fG} = 0.6$ in S-glass/epoxy lamina, and $V_{fG} = 0.3$ and $V_{fPP} = 0.3$ in S-glass/PP/epoxy) is considered, and the fibres have the same diameter (10 μm). The middle fibre is used to introduce eccentricity (see Fig. 1) by varying the angle ($\theta_e = 0°$, 45°, and 90°), and the distance ($\delta_e = 0.2R$, where R represents the fibre radius). Figure 7 shows the normalized von Mises matrix stress under transverse tension (*i.e.,* $\sigma_{vM}/\widehat{\sigma}_{22}$) for the non-eccentric and eccentric cases for S-glass/epoxy and S-glass/PP/epoxy. Figure 7a–d show that the normalised matrix stress distribution is significantly affected by fibre eccentricity in non-hybrid S-glass/epoxy lamina. The maximum normalised stress increases with decreasing inter-fibre distance. The highest normalised stress is thus induced, with $\delta_e = 0.2R$ and $\theta_e = 45°$ (Fig. 7c), which is ~ 90% higher than the maximum normalised stress occurred without eccentricity (Fig. 7a).

Next, Fig. 7e–h show that the normalised matrix stress distribution is only marginally affected by fibre eccentricity in fibre-hybrid S-glass/PP/epoxy lamina as the middle (secondary) fibre stiffness is significantly lower than that of the corner (S-glass) fibre. Although the maximum normalised stress increases with decreasing inter-fibre distance, the highest normalised stress, with $\delta_e = 0.2R$ and $\theta_e = 45°$ (Fig. 7g), is only ~ 6% higher than the maximum normalised stress occurred without fibre eccentricity (Fig. 7e).

Figures 8 and 9 show the normalized normal stress ($\sigma_n/\widehat{\sigma}_{22}$) and shear stress ($\tau_{nt}/\widehat{\sigma}_{22}$) distribution at S-glass and PP fibre interfaces under transverse tension for S-glass/epoxy and S-glass/PP/epoxy laminae. First, from Fig. 8a, where the normalised normal stress distribution at S-glass fibre interface is shown, it is seen that the fibre eccentricity can significantly increase the interfacial normal stress in non-hybrid S-glass/epoxy as the inter-fibre distance between the high stiffness fibres is decreased, aligning with the loading direction. When the eccentricity angle is set to $\theta_e = 45°$ and 90°, a substantial rise in the normal stress is observed, reaching a peak of ~ 1.4 at $\theta = 45°$ for $\theta_e = 90°$ and $\delta_e = 0.2R$. This is an increase of ~ 90% compared to the normal stress without fibre eccentricity (*i.e.,* centred). In contrast, for fibre-hybrid S-glass/PP/lamina, as seen Fig. 8b–c, where the normalised normal stress distributions at S-glass and PP fibre interfaces are shown, the fibre eccentricity has negligible influence on the interfacial normal stress distribution because of the low stiffness of the middle PP fibre. Next, from Fig. 9a, it is evident that the fibre eccentricity significantly affects the normalised shear stress distribution at S-glass fibre in S-glass/epoxy lamina. But the maximum $\tau_{nt}/\widehat{\sigma}_{22}$ is observed at $\theta = 45°$ for $\theta_e = 45°$ and $\delta_e = 0.2R$. The increase is ~ 85% compared to that of the baseline (without eccentricity). For fibre-hybrid S-glass/PP/epoxy lamina, no significant variation is observed for $\sigma_n/\widehat{\sigma}_{22}$ and $\tau_{nt}/\widehat{\sigma}_{22}$, where the eccentric middle fibre is the PP (low-stiffness) fibre (see Fig. 9b, c).

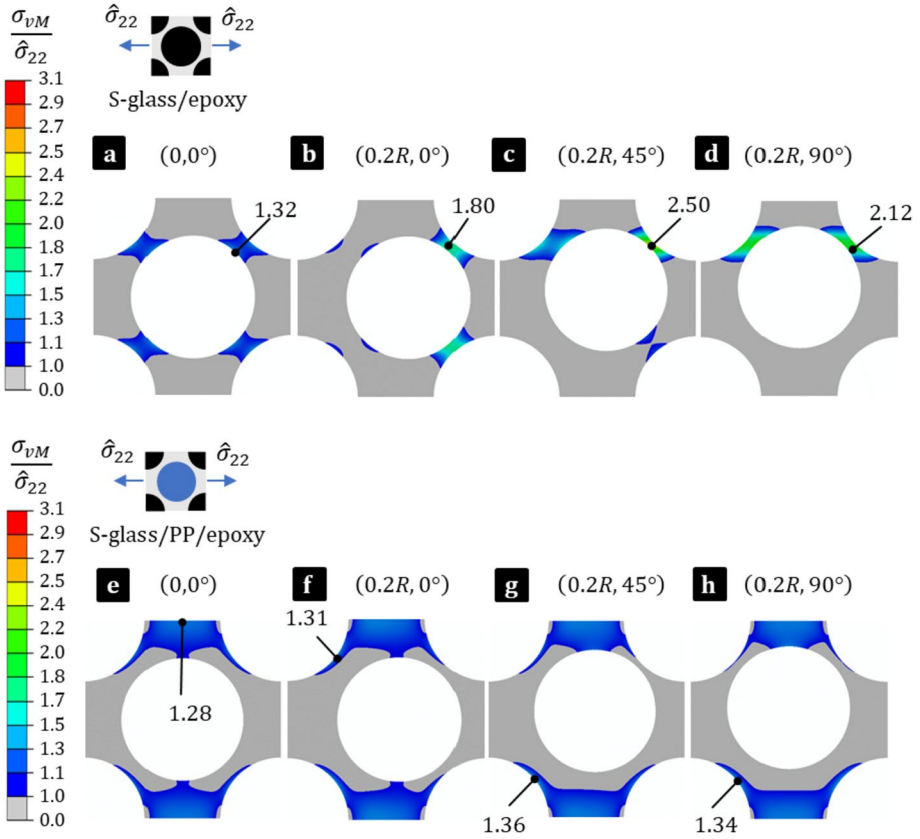

Fig. 7 The normalised von Mises matrix stress under transverse tension due to middle fibre eccentricity: **a** S-glass/epoxy centred, S-glass/epoxy with fibre eccentricity at **b** 0°, **c** 45°, **d** 90°, and **e** S-glass/PP/epoxy centred, S-glass/PP/epoxy with fibre eccentricity at **f** 0°, **g** 45°, and **h** 90°

3.2.3 The Effect of Fibre Eccentricity on Micro-stress Fields Under Transverse Shear

The effect of fibre eccentricity is studied in non-hybrid S-glass/epoxy and fibre-hybrid S-glass/PP/epoxy laminae with a total fibre volume fraction of 0.6 (*i.e.*, $V_{fG} = 0.6$ in S-glass/epoxy lamina, and $V_{fG} = 0.3$ and $V_{fPP} = 0.3$ in S-glass/PP/epoxy). Figure 10 shows the normalized von Mises matrix stress under transverse shear (*i.e.*, $\sigma_{vM}/\hat{\sigma}_{23}$) for the non-eccentric and eccentric cases for S-glass/epoxy and S-glass/PP/epoxy. Figure 10a–d show that the normalised matrix stress distribution is considerably altered by fibre eccentricity in non-hybrid S-glass/epoxy lamina. The highest normalised matrix stress is induced with fibre eccentricity ($\delta_e = 0.2R$ and $\theta_e = 45°$), is ~ 20% higher than the maximum normalised stress occurred without eccentricity (Fig. 10a). Next, Fig. 10e–h show that the normalised matrix stress distribution is also considerably affected by fibre eccentricity in fibre-hybrid S-glass/PP/epoxy lamina. By comparing the matrix stress distributions in S-glass/epoxy (Fig. 10a–d) and S-glass/PP/epoxy (Fig. 10e–h), it is evident that the $\sigma_{vM}/\hat{\sigma}_{23}$ stress peak in S-glass/PP/epoxy is significantly higher (~ 80%) higher than that in S-glass/epoxy. It is also seen that the eccentricity angle, which is observed to have a significant effect under

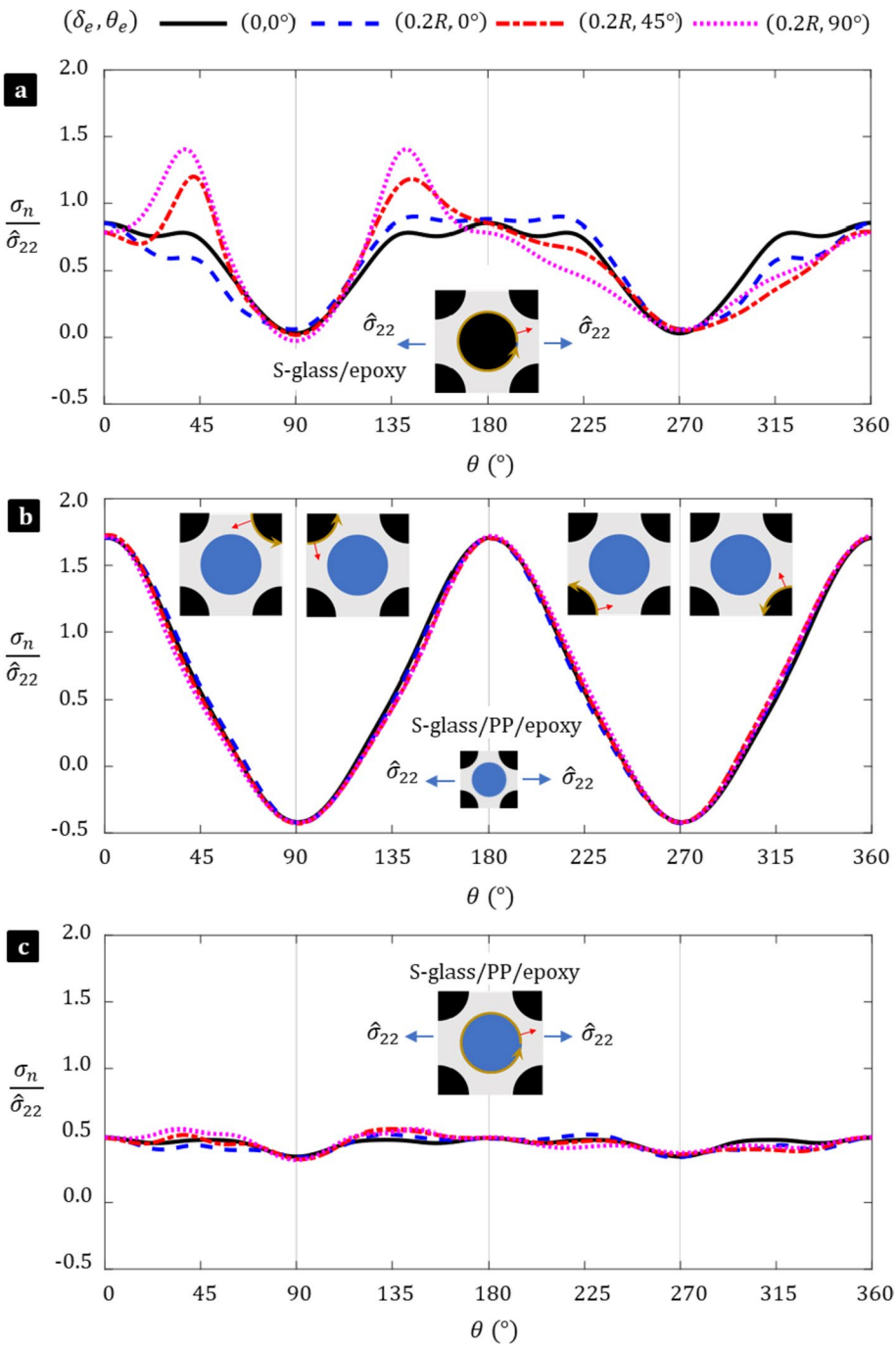

Fig. 8 Interface stress study: **a** normalised interfacial normal stress for the S-glass fibre in S-glass/epoxy, **b** S-glass fibre in S-glass/PP/epoxy, and **c** S-glass fibre in S-glass/PP/epoxy

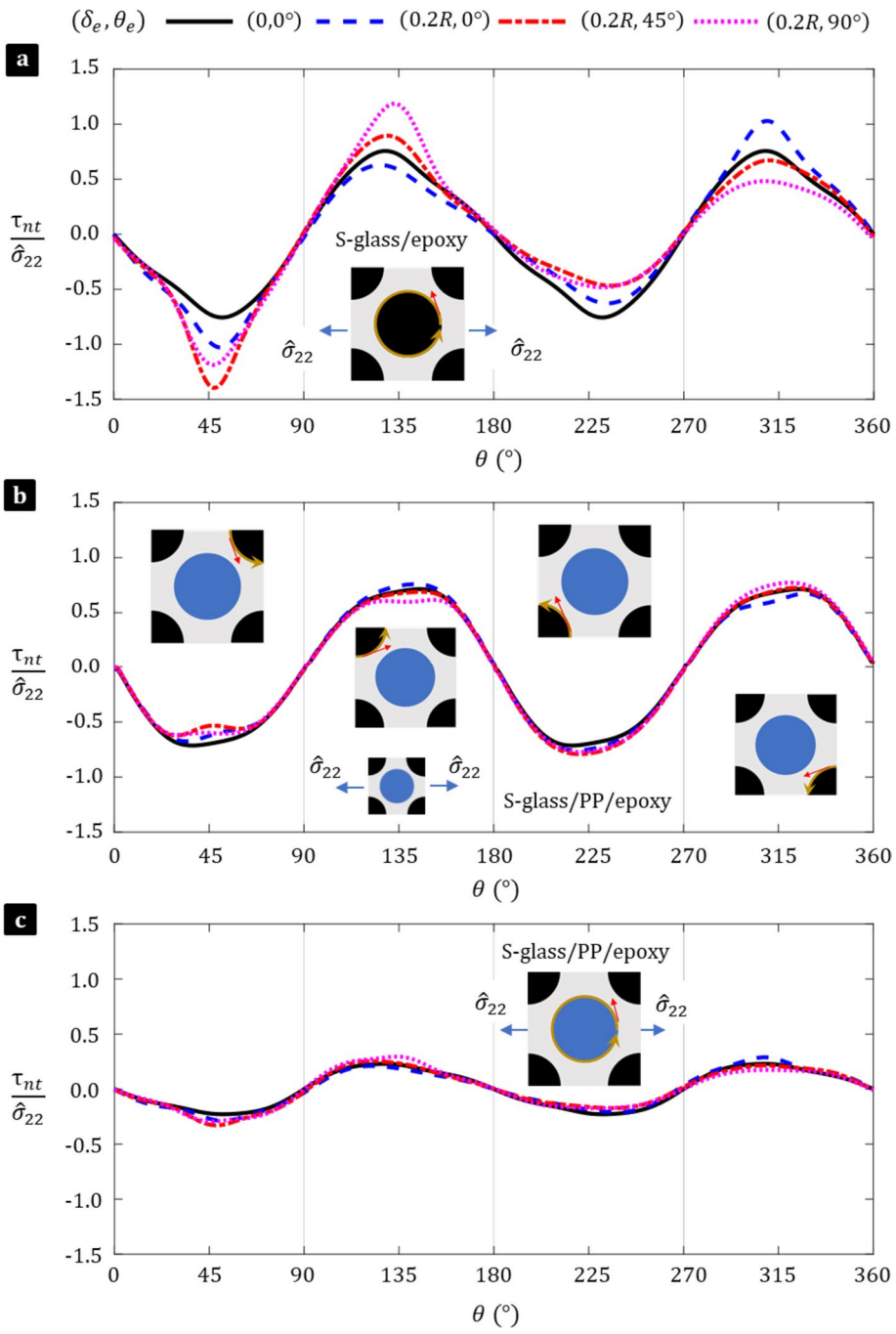

Fig. 9 Interface stress study: **a** normalised interfacial shear stress for the S-glass fibre in S-glass/epoxy, **b** S-glass fibre in S-glass/PP/epoxy, and **c** S-glass fibre in S-glass/PP/epoxy

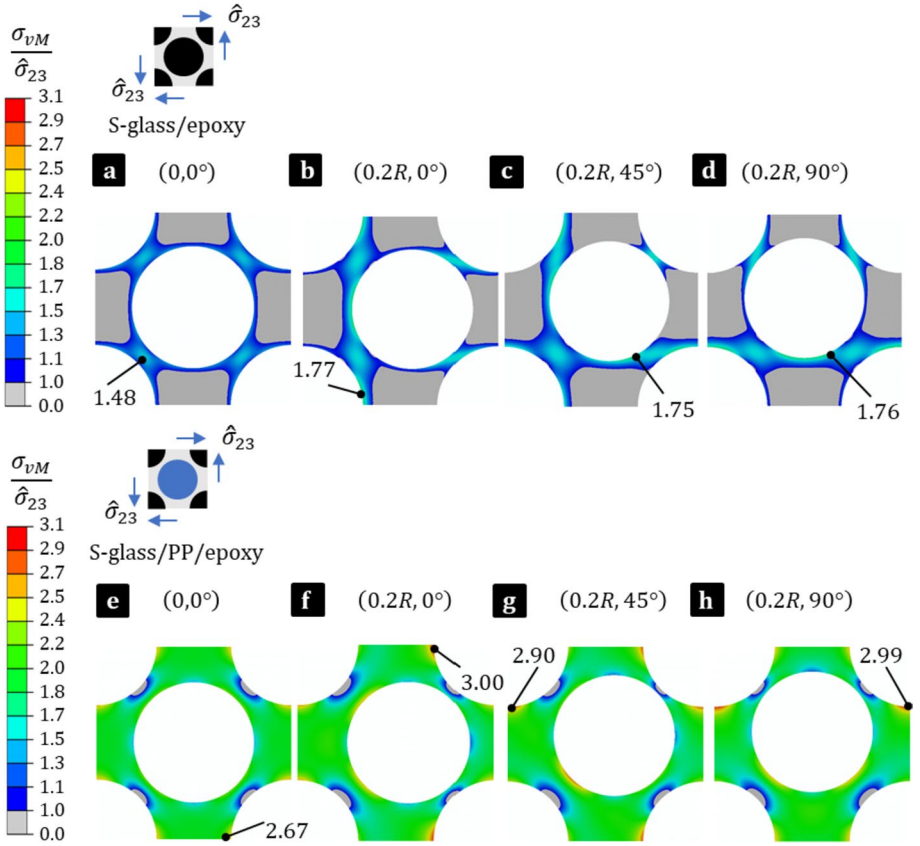

Fig. 10 The normalised von Mises matrix stress due to middle fibre eccentricity under transverse shear: **a** S-glass/epoxy centred, S-glass/epoxy with fibre eccentricity at **b** 0°, **c** 45°, **d** 90°, and **e** S-glass/PP/epoxy centred, S-glass/PP/epoxy with fibre eccentricity at **f** 0°, **g** 45°, and **h** 90°

transverse tension, has only a marginal role under transverse shear (comparing Figs. 7 and 10) When the fibre is eccentric the increase in stress peak compared to the base case is ~ 20%. Thus, under transverse shear, the von Mises matrix stress distribution is highly influenced by the inter-fibre distance, but not by the eccentricity angle.

Figures 11 and 12 show the normalized normal stress ($\sigma_n/\hat{\sigma}_{23}$) and shear stress ($\tau_{nt}/\hat{\sigma}_{23}$) distribution at S-glass and PP fibre interfaces under transverse shear for S-glass/epoxy and S-glass/PP/epoxy laminae. First, from Fig. 11a, where the normalised normal stress distribution at S-glass fibre interface is shown, it is seen that the fibre eccentricity can considerably increase the interfacial normal stress in non-hybrid S-glass/epoxy as the inter-fibre distance between the high stiffness fibres is decreased. When the eccentricity is set to $\theta_e = 45°$ and $\delta_e = 0.2R$, a significant rise in the normal stress is observed, reaching a peak of ~ 3.2, which is an increase of ~ 50% compared to the normal stress without fibre eccentricity (*i.e.,* centred). In contrast, for fibre-hybrid S-glass/PP/lamina, as seen Fig. 11b, c, where the normalised normal stress distributions at S-glass and PP fibre interfaces are shown, the fibre eccentricity has negligible influence on the interfacial normal stress distribution because of the low stiffness of the middle PP fibre. Next, from Fig. 12a, it is evident

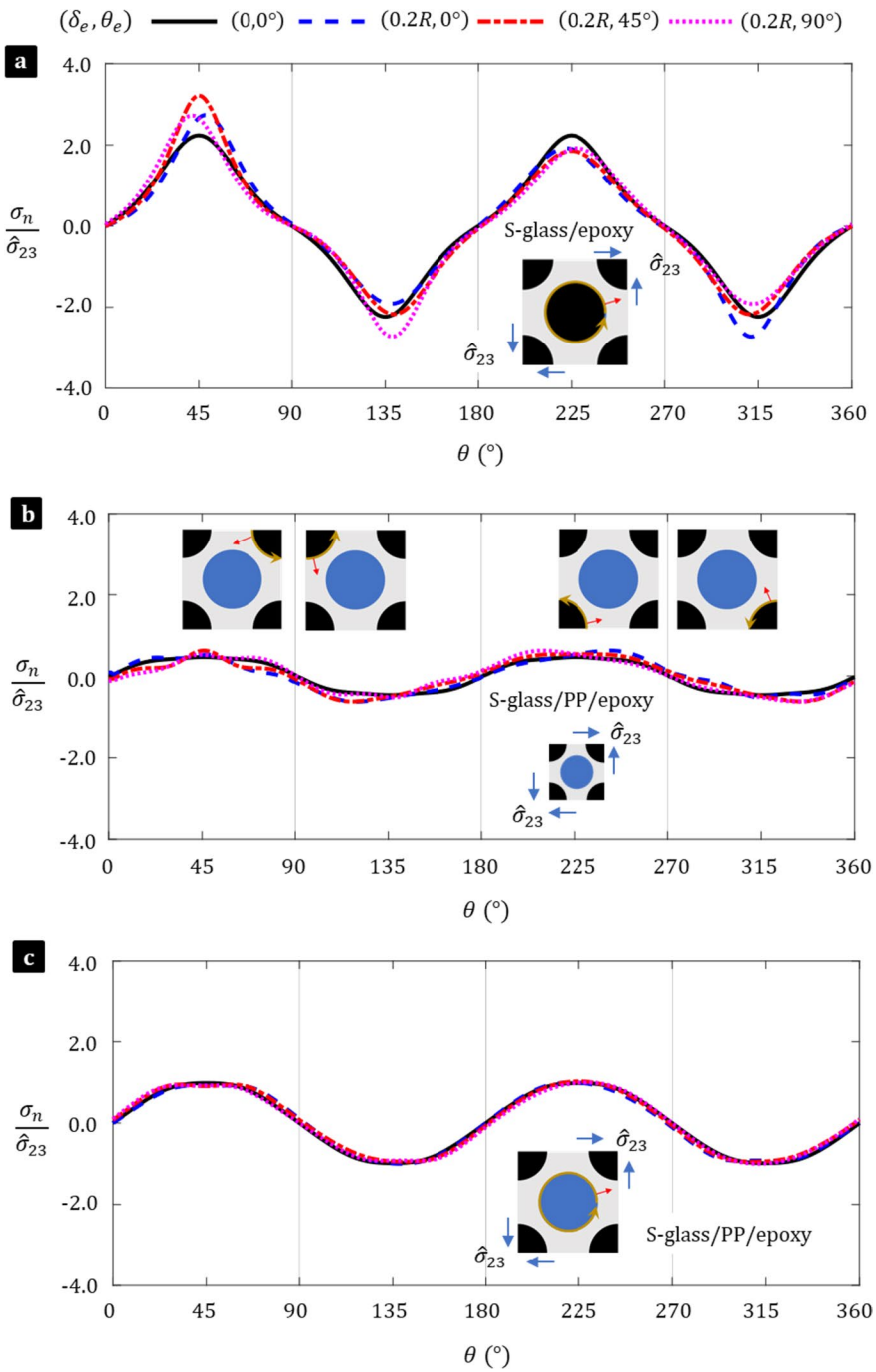

Fig. 11 The normalised interfacial normal stress for different eccentricity angles and distances for S-glass/epoxy and S-glass/PP/epoxy under transverse shear: **a** the S-glass fibre in S-glass/epoxy, **b** S-glass fibre in S-glass/PP/epoxy, and **c** S-glass fibre in S-glass/PP/epoxy

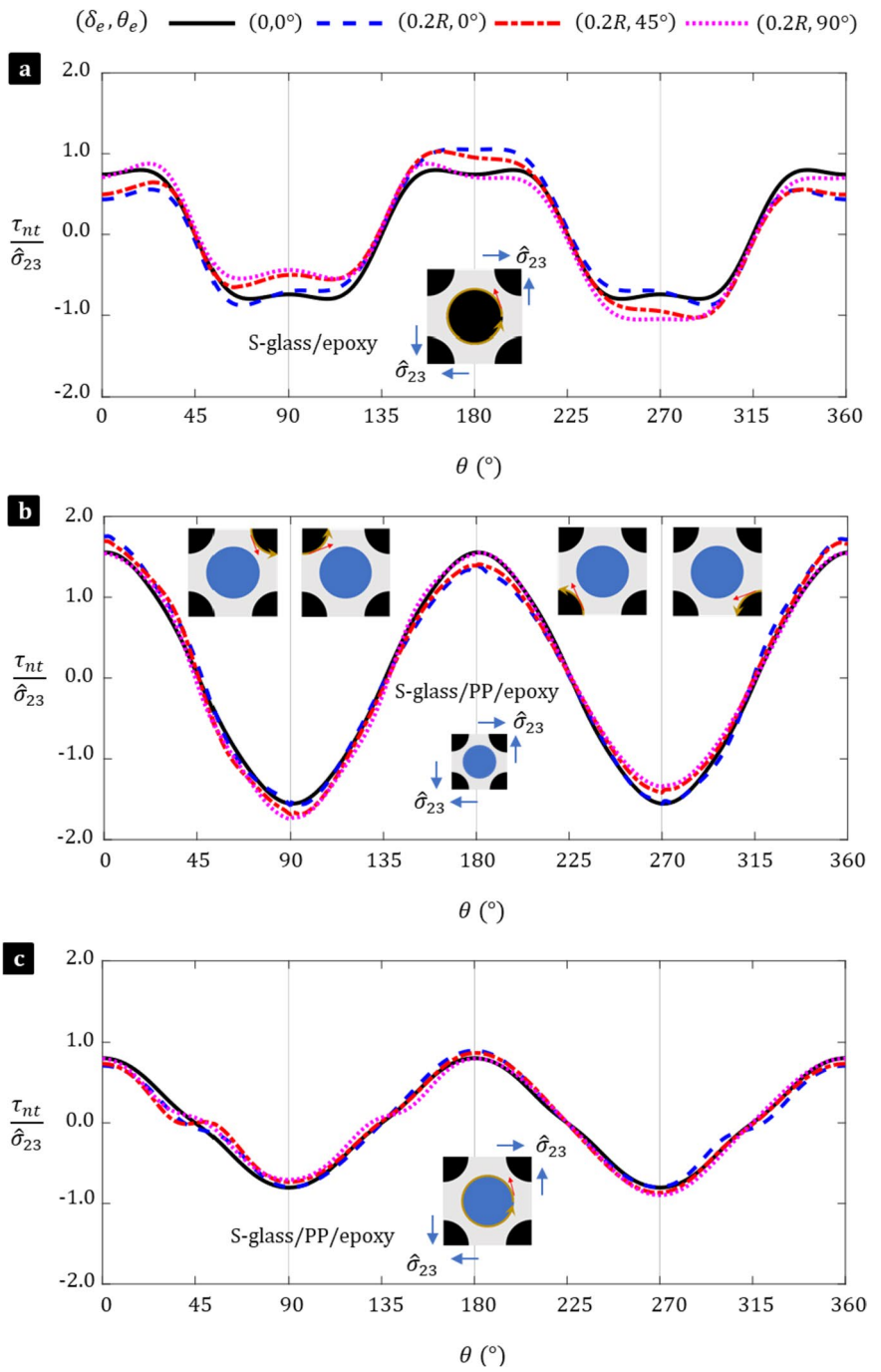

Fig. 12 The normalised interfacial shear stresses for different eccentricity angles and distances for S-glass/epoxy and S-glass/PP/epoxy under transverse shear: **a** S-glass fibre in S-glass/epoxy, **b** S-glass fibre in S-glass/PP/epoxy, and (**c**) S-glass fibre in S-glass/PP/epoxy

that the fibre eccentricity considerably affects the normalised shear stress distribution at S-glass fibre in S-glass/epoxy lamina. For fibre-hybrid S-glass/PP/epoxy lamina, no significant variation is observed for $\sigma_n/\widehat{\sigma}_{23}$ and $\tau_{nt}/\widehat{\sigma}_{23}$, where the eccentric middle fibre is the PP (low-stiffness) fibre (see Fig. 12b, c).

4 Conclusions

This study is focused on the effect of intra-laminar fibre hybridisation, *i.e.,* primary and secondary fibres within a matrix, on the homogenised properties and micro-stress fields in uni-directional polymer composite laminae. A 2D RUC model with periodic microstructure is employed to conduct the micro-mechanical analyses under transverse tensile and shear loading–with an emphasis on the matrix-dominant responses. Uni-directional fibre-hybrid S-glass/epoxy laminae with different secondary fibres are investigated to understand the effect of fibre hybridisation and fibre eccentricity (inter-fibre distance) on the intra-lamina micro-stress fields (*i.e.,* matrix and fibre-matrix interface stress distribution). As expected, it is observed that the homogenised elastic lamina properties can be significantly altered via intra-lamina fibre hybridisation. The effective density and thus specific elastic moduli of unidirectional lamina can be tailored by introducing secondary fibres with varying stiffness and density. However, the matrix-dominant response of fibre-hybrid lamina under transverse tension and transverse shear conditions show that the micro-stress fields (within the matrix and at the primary and secondary fibre-matrix interfaces) can significantly be altered depending on the stiffness of the secondary fibre, especially when the stiffness of the secondary fibre is close to or less than that of the matrix. Moreover, the micro-stress fields are observed to be sensitive to fibre eccentricities (inter-fibre distance) when the stiffness of the secondary fibre is close to or higher than that of the primary fibre. In contrast, the effect of fibre eccentricities is found to be insignificant when the stiffness of the secondary fibre is considerably less than that of the primary fibre. In the case of S-glass/PP/epoxy lamina, the presence of the secondary PP fibre with a significantly lower stiffness ($E_{fS} = 1.74$ GPa), compared to the primary (S-glass) fibre ($E_{fG} = 87$ GPa) and the matrix ($E_m = 2.55$ GPa), is seen to induce a large increase in the normalised matrix stress under transverse tension as well as transverse shear conditions, when compared to that of the baseline (S-glass/epoxy lamina). When the secondary fibre stiffness is higher than that of the matrix ($E_{fS} = 8.7$ GPa), but lower than that of the primary (S-glass) fibre, it is seen to redistribute the matrix stresses and consequently reduce the normalised peak matrix stress. In general, the observations made emphasize the importance of the secondary fibre stiffness in tailoring the macroscopic elastic lamina properties and the microscopic behaviour of fibre-hybrid lamina–and thus on the mechanical behaviour of such intra-laminar fibre-hybrid laminates. As the micro-stress fields within the matrix and at primary and secondary fibre-matrix interfaces are seen to be sensitive to fibre hybridisation, composite laminates with intra-laminar hybridisation could alter damage initiation and propagation mechanisms and could provide opportunities for tailoring damage tolerance and energy dissipation.

Acknowledgements We would like to acknowledge the Department of Mechanical, Aerospace, and Civil Engineering at The University of Manchester for granting a scholarship to support this research.

Author Contributions Giuseppe Romano: Investigation, Conceptualization, Methodology, Visualization, Writing – original draft. Yeshwanth Nagaraja Rao: Conceptualization, Writing – review & editing. Chengguang Liu: Conceptualization, Writing – review & editing. Kali-Babu Katnam: Conceptualization, Supervision, Writing

– review & editing. Zhenmin Zou: Conceptualization, Supervision, Writing – review & editing. Prasad Potluri: Supervision, Writing – review & editing.

Funding Departmental Award (MACE strategic support studentship).

Data Availability The data produced and examined throughout this study can be provided upon request to the lead author.

Declarations

Conflict of Interests The authors declare no competing interests.

References

1. Richardson, M.O.W., Wisheart, M.J.: Review of low-velocity impact properties of composite materials. Compos. A Appl. Sci. Manuf. **27**, 1123–1131 (1996). https://doi.org/10.1016/1359-835X(96)00074-7
2. Bernet, N., Michaud, V., Bourban, P.-E., Månson, J.-A.E.: Commingled yarn composites for rapid processing of complex shapes. Compos. A Appl. Sci. Manuf. **32**, 1613–1626 (2001). https://doi.org/10.1016/S1359-835X(00)00180-9
3. Hufenbach, W., Böhm, R., Thieme, M., Winkler, A., Mäder, E., Rausch, J., Schade, M.: Polypropylene/glass fibre 3D-textile reinforced composites for automotive applications. Mater. Des. **32**, 1468–1476 (2011). https://doi.org/10.1016/j.matdes.2010.08.049
4. Trudel-Boucher, D., Fisa, B., Denault, J., Gagnon, P.: Experimental investigation of stamp forming of unconsolidated commingled E-glass/polypropylene fabrics. Compos. Sci. Technol. **66**, 555–570 (2006). https://doi.org/10.1016/j.compscitech.2005.05.036
5. Vieille, B., Casado, V.M., Bouvet, C.: About the impact behavior of woven-ply carbon fiber-reinforced thermoplastic- and thermosetting-composites: A comparative study. Compos. Struct. **101**, 9–21 (2013). https://doi.org/10.1016/j.compstruct.2013.01.025
6. Shah, S.Z.H., Karuppanan, S., Megat-Yusoff, P.S.M., Sajid, Z.: Impact resistance and damage tolerance of fiber reinforced composites: A review. Compos. Struct. **217**, 100–121 (2019). https://doi.org/10.1016/j.compstruct.2019.03.021
7. Mazumdar, S. (2001). Composites Manufacturing: Materials, Product, and Process Engineering (1st ed.). CRC Press. https://doi.org/10.1201/9781420041989
8. Chamis, C., Lark, R.: Hybrid composites - State-of-the-art review: Analysis, design, application and fabrication, in 18th Structural Dynamics and Materials Conference, American Institute of Aeronautics and Astronautics. https://doi.org/10.2514/6.1977-415
9. Swolfs, Y., Gorbatikh, L., Verpoest, I.: Fibre hybridisation in polymer composites: A review. Compos. A Appl. Sci. Manuf. **67**, 181–200 (2014). https://doi.org/10.1016/j.compositesa.2014.08.027
10. Swolfs, Y., Verpoest, I., Gorbatikh, L.: Recent advances in fibre-hybrid composites: materials selection, opportunities and applications. Int. Mater. Rev. **64**, 181–215 (2019). https://doi.org/10.1080/09506608.2018.1467365
11. Selver, E., Potluri, P., Hogg, P., Soutis, C.: Impact damage tolerance of thermoset composites reinforced with hybrid commingled yarns. Compos. B Eng. **91**, 522–538 (2016). https://doi.org/10.1016/j.compositesb.2015.12.035
12. Selver, E., Potluri, P.: Intra-tow micro-wrapping for damage tolerance. Compos. Sci. Technol. **213**, 108935 (2021). https://doi.org/10.1016/j.compscitech.2021.108935

13. Dalfi, H., Katnam, K.B., Potluri, P.: Intra-laminar toughening mechanisms to enhance impact damage tolerance of 2D woven composite laminates via yarn-level fiber hybridization and fiber architecture. Polym. Compos. **40**, 4573–4587 (2019). https://doi.org/10.1002/pc.25325
14. Katnam, K.B., Dalfi, H., Potluri, P.: Towards balancing in-plane mechanical properties and impact damage tolerance of composite laminates using quasi-UD woven fabrics with hybrid warp yarns. Compos. Struct. **225**, 111083 (2019). https://doi.org/10.1016/j.compstruct.2019.111083
15. Ritchie, R.O.: The conflicts between strength and toughness. Nat. Mater. **10**, 817–822 (2011). https://doi.org/10.1038/nmat3115
16. Mäder, E., Rausch, J., Schmidt, N.: Commingled yarns – Processing aspects and tailored surfaces of polypropylene/glass composites. Compos. A Appl. Sci. Manuf. **39**, 612–623 (2008). https://doi.org/10.1016/j.compositesa.2007.07.011
17. Sun, Q., Meng, Z., Zhou, G., Lin, S.-P., Kang, H., Keten, S., Guo, H., Su, X.: Multi-scale computational analysis of unidirectional carbon fiber reinforced polymer composites under various loading conditions. Compos. Struct. **196**, 30–43 (2018). https://doi.org/10.1016/j.compstruct.2018.05.025
18. Ma, Y., Yang, Y., Sugahara, T., Hamada, H.: A study on the failure behavior and mechanical properties of unidirectional fiber reinforced thermosetting and thermoplastic composites. Compos. B Eng. **99**, 162–172 (2016). https://doi.org/10.1016/j.compositesb.2016.06.005
19. Chevalier, J., Camanho, P.P., Lani, F., Pardoen, T.: Multi-scale characterization and modelling of the transverse compression response of unidirectional carbon fiber reinforced epoxy. Compos. Struct. **209**, 160–176 (2019). https://doi.org/10.1016/j.compstruct.2018.10.076
20. Xia, Z., Zhang, Y., Ellyin, F.: A unified periodical boundary conditions for representative volume elements of composites and applications. Int. J. Solids Struct. **40**, 1907–1921 (2003). https://doi.org/10.1016/S0020-7683(03)00024-6
21. Sun, C.T., Vaidya, R.S.: Prediction of composite properties from a representative volume element. Compos. Sci. Technol. **56**, 171–179 (1996). https://doi.org/10.1016/0266-3538(95)00141-7
22. Li, S.: General unit cells for micromechanical analyses of unidirectional composites. Compos. A Appl. Sci. Manuf. **32**, 815–826 (2001). https://doi.org/10.1016/S1359-835X(00)00182-2
23. Hojo, M., Mizuno, M., Hobbiebrunken, T., Adachi, T., Tanaka, M., Ha, S.K.: Effect of fiber array irregularities on microscopic interfacial normal stress states of transversely loaded UD-CFRP from viewpoint of failure initiation. Compos. Sci. Technol. **69**, 1726–1734 (2009). https://doi.org/10.1016/j.compscitech.2008.08.032
24. Jin, K.K., Oh, J.H., Ha, S.K.: Effect of fiber arrangement on residual thermal stress distributions in a unidirectional composite. J. Compos. Mater. **41**, 591–611 (2007). https://doi.org/10.1177/0021998306065290
25. Babu, K.S., Rao, K.M., Raju, V. et al.: Micromechanical analysis of FRP hybrid composite lamina for in-plane transverse loading. Indian J Eng. Mater. Sci. **15**, 382–395 (2008). http://nopr.niscpr.res.in/handle/123456789/2588
26. Banerjee, S., Sankar, B.V.: Mechanical properties of hybrid composites using finite element method based micromechanics. Compos. B Eng. **58**, 318–327 (2014). https://doi.org/10.1016/j.compositesb.2013.10.065
27. Vignoli, L.L., Savi, M.A., Pacheco, P.M.C.L., Kalamkarov, A.L.: Comparative analysis of micromechanical models for the elastic composite laminae. Compos. B Eng. **174**, 106961 (2019). https://doi.org/10.1016/j.compositesb.2019.106961
28. Abaimov, S.G., Khudyakova, A.A., Lomov, S.V.: On the closed form expression of the Mori-Tanaka theory prediction for the engineering constants of a unidirectional fiber-reinforced ply. Compos. Struct. **142**, 1–6 (2016). https://doi.org/10.1016/j.compstruct.2016.02.001
29. Benveniste, Y.: A new approach to the application of Mori-Tanaka's theory in composite materials. Mech. Mater. **6**, 147–157 (1987). https://doi.org/10.1016/0167-6636(87)90005-6
30. Gibson, R.F. (2007). Principles of Composite Material Mechanics (2nd ed.). CRC Press. https://doi.org/10.1201/9781420014242
31. Hopkins, D.A., Chamis, C.C.: A unique set of micromechanics equations for high-temperature metal matrix composites. Test. Technol. Metal Matrix Compos. (1988). https://doi.org/10.1520/STP25950S
32. Aboudi, J., Arnold, S.M., Bednarcyk, B.A.: The method of cells micromechanics. In: Micromechanics of Composite Materials. pp. 147–226. Elsevier. (2013). Hardback ISBN: 9780123970350970123970350, Paperback ISBN: 9780128101278978012810127 8, eBook ISBN: 9780123977595
33. Younes, R. et al.: Comparative Review Study on Elastic Properties Modeling for Unidirectional Composite Materials, in Composites and Their Properties, IntechOpen. (2012). https://doi.org/10.5772/50362
34. Mallick, P.K. (2007). Fiber-Reinforced Composites: Materials, Manufacturing, and Design, Third Edition (3rd ed.). CRC Press. https://doi.org/10.1201/9781420005981
35. Daniel, I.M., Ishai, O.: Engineering mechanics of composite materials. Oxford University Press, New York (2006), ISBN 978-0-19-515097-1
36. Wypych, G.: Handbook of polymers. ChemTec Publishing, Toronto (2016), ISBN 978-1-927885-96-3

37. Osswald, T.A. (ed.): International plastics handbook: the resource for plastics engineers. Hanser, Munich, Cincinnati. (2006). ISBN 3-446-22905-1
38. 'Araldite LY 564 : Aradur 2954', Mouldlife. Accessed: Feb. 25, 2024. [Online]. Available: https://www.mouldlife.net/araldite--ly-1564--aradur--2954-1414-p.asp
39. D'Mello, R.J., Waas, A.M.: Virtual curing of textile polymer matrix composites. Compos. Struct. **178**, 455–466 (2017). https://doi.org/10.1016/j.compstruct.2017.05.045
40. Zhou, L., Chen, M., Liu, C., Wu, H.: A multi-scale stochastic fracture model for characterizing the tensile behavior of 2D woven composites. Compos. Struct. **204**, 536–547 (2018). https://doi.org/10.1016/j.compstruct.2018.07.128
41. Vaughan, T.J., McCarthy, C.T.: A micromechanical study on the effect of intra-ply properties on transverse shear fracture in fibre reinforced composites. Compos. A Appl. Sci. Manuf. **42**, 1217–1228 (2011). https://doi.org/10.1016/j.compositesa.2011.05.004
42. Vaughan, T.J., McCarthy, C.T.: Micromechanical modelling of the transverse damage behaviour in fibre reinforced composites. Compos. Sci. Technol. **71**, 388–396 (2011). https://doi.org/10.1016/j.compscitech.2010.12.006
43. Yang, L., Yan, Y., Ran, Z., Liu, Y.: A new method for generating random fibre distributions for fibre reinforced composites. Compos. Sci. Technol. **76**, 14–20 (2013). https://doi.org/10.1016/j.compscitech.2012.12.001
44. Al-Ostaz, A., Jasiuk, I.: Crack initiation and propagation in materials with randomly distributed holes. Eng. Fract. Mech. **58**, 395–420 (1997). https://doi.org/10.1016/S0013-7944(97)00039-8
45. Okereke, M.I., Akpoyomare, A.I.: A virtual framework for prediction of full-field elastic response of unidirectional composites. Comput. Mater. Sci. **70**, 82–99 (2013). https://doi.org/10.1016/j.commatsci.2012.12.036
46. Li, S., Sitnikova, E.: Representative volume elements and unit cells. In: Representative Volume Elements and Unit Cells. pp. 67–77. Elsevier. (2020). https://doi.org/10.1016/C2017-0-03559-0. ISBN 978-0-08-102638-0
47. Sádaba, S., Herráez, M., Naya, F., González, C., Llorca, J., Lopes, C.S.: Special-purpose elements to impose Periodic Boundary Conditions for multiscale computational homogenization of composite materials with the explicit finite element method. Compos. Struct. **208**, 434–441 (2019). https://doi.org/10.1016/j.compstruct.2018.10.037